Locally parity-time-symmetric and globally parity-symmetric systems

W. W. Ahmed,[1] R. Herrero,[1] M. Botey,[1] and K. Staliunas[1,2]
[1]*Departament de Física, Universitat Politècnica de Catalunya (UPC), Colom 11, E-08222 Terrassa, Barcelona, Spain*
[2]*Institució Catalana de Recerca i Estudis Avançats (ICREA), Passeig Lluís Companys 23, E-08010 Barcelona, Spain*
(Received 3 May 2016; published 11 November 2016)

We introduce a class of systems holding parity-time ($\mathcal{PT}$) symmetry locally, whereas being globally $\mathcal{P}$ symmetric. The potential, $U = U(|r|)$, fulfills $\mathcal{PT}$ symmetry with respect to periodically distributed points $r_0 : U(|r_0 + r|) = U^*(|r_0 - r|)$ being $r_0 \neq 0$. We show that such systems hold unusual properties arising from the merging of the two different symmetries, leading to a strong field localization and enhancement at the double-symmetry center, $r = 0$, when the coupling of outward to inward propagating waves is favored. We explore such general potentials in one and two dimensions, which could have actual realizations combining gain-loss and index modulations in nanophotonic structures. In particular, we show how to render a broad aperture vertical-cavity surface-emitting laser into a bright and narrow beam source, as a direct application.

DOI: 10.1103/PhysRevA.94.053819

I. INTRODUCTION

$\mathcal{PT}$-symmetric systems, introduced as a curiosity in quantum mechanics [1,2], are recently being explored in the field of acoustics [3], plasmonics [4], or Bose-Einstein condensates [5] and more extensively in optics [6–8]. A necessary condition for a system to be $\mathcal{PT}$ symmetric is that the complex potential fulfills $U(r) = U^*(-r)$. Therefore, in the case of periodic $\mathcal{PT}$-symmetric systems, the requirement is that the real and complex modulations of the potential are dephased a quarter of the period of the modulation. While being complex, such systems may have real spectra and hold counterintuitive physical effects arising from their complex topology. Depending on parameters, above some threshold value, the $\mathcal{PT}$ symmetry may be spontaneously broken, the eigenvalues become complex conjugate pairs, and a phase transition occurs at this exceptional point (EP). This is the onset of the so-called $\mathcal{PT}$-phase transition leading to unusual features. Among these novel unexpected properties are asymmetric reflections, asymmetric invisibility, asymmetric mode coupling, Bloch oscillations, spectral singularities, or coherent perfect absorbers as time-reversed lasers [9–13].

However, most periodic $\mathcal{PT}$-symmetric systems can be regarded as belonging to two limiting situations corresponding to already well-known potentials. On one extreme, there are purely real-valued periodic potentials, which in the simplest harmonic modulation case may be expressed as $U(r) = n_{\mathrm{Re}}\cos(qx)$, being q the spatial period of the modulation and n_{Re} its amplitude. On the other extreme, there are purely imaginary potentials exhibiting gain-loss modulations, which in the simplest harmonic case may be simply expressed as $U(r) = n_{\mathrm{Im}}\cos(qx)$. Note that both limits lead to a symmetric coupling of resonant modes, i.e., the two counterpropagating modes with wave vector $|k|$, $\exp(-ikx)$ and $\exp(ikx)$, are coupled symmetrically at resonance, for $q = 2k$. The peculiar situation arises close to the EP, only when both the real and imaginary parts of the potential are simultaneously modulated, with a $\pm\pi/2$ phase shift: $U(r) = n_{\mathrm{Re}}\cos(qx) + in_{\mathrm{Im}}\sin(qx)$. Indeed, when both modulations are balanced, $n_{\mathrm{Re}} = n_{\mathrm{Im}}$, the complex potential can be simply expressed as $U(r) = n\exp(\pm iqx)$, which evidences that the coupling becomes strongly unidirectional. For example, for such a complex modulation the left-propagating mode $\exp(-ikx)$, is efficiently coupled to the right propagating mode, $\exp(+ikx)$, but not vice versa. The point $n_{\mathrm{Re}} = n_{\mathrm{Im}}$ is precisely the EP or PT-phase transition, separating two extreme situations. Mathematically, the coupling between the two, left/right, propagating mode is conveniently described via linear coupling matrices, $M = \{\{0, n_{\mathrm{Re}} + n_{\mathrm{Im}}\}, \{n_{\mathrm{Re}} - n_{\mathrm{Im}}, 0\}\}$, which at the $\mathcal{PT}$-phase transition point degenerate to $M = \{\{0, 2n\}, \{0, 0\}\}$. Generally, in the presence of more modes (or mode continuum) the description of the field dynamics becomes more complex; however, the phase transition separating the two extreme limits of real-like and imaginary-like periodic potentials still exists. The question that arises is what occurs if the $\mathcal{PT}$-symmetry condition is not met globally but only locally. Let us consider a simple one-dimensional (1D) situation as the one represented in Fig. 1(a): such a complex potential leads to a unidirectional coupling "to the left" on the right half-space, and "to the right" on the left half-space. Therefore, an accumulation of the field can be expected at $x = 0$. The same idea applies to two dimensions (2D) [see Figs. 1(b) and 1(d)], when the radial coupling between incoming and outgoing axisymmetric waves is asymmetric. Note that the physical realizations of the two above discussed arrangements, in 1D and 2D, are nowadays available in microphotonics, in particular for the special fabrication of microchip and vertical-cavity surface-emitting lasers (VCSELs) [14,15]. In optics, the refractive index corresponds to the real component of the potential, whereas gain or loss stands for its imaginary part; purely real or imaginary modulated systems being photonic crystals and gain-loss modulated (GLM) systems, respectively [16–20]. Therefore, $\mathcal{PT}$-symmetric optical potentials are expected to behave either as PhC-like systems or as GLM-like systems.

In this article, we propose a class of locally $\mathcal{PT}$-symmetric and globally $\mathcal{P}$-symmetric systems for field localization and enhancement, which we analyze on general linear systems both in 1D and in 2D. To show the potential application of the idea, we explore a specific nonlinear system, the 2D VCSEL, in the concluding part of the article.

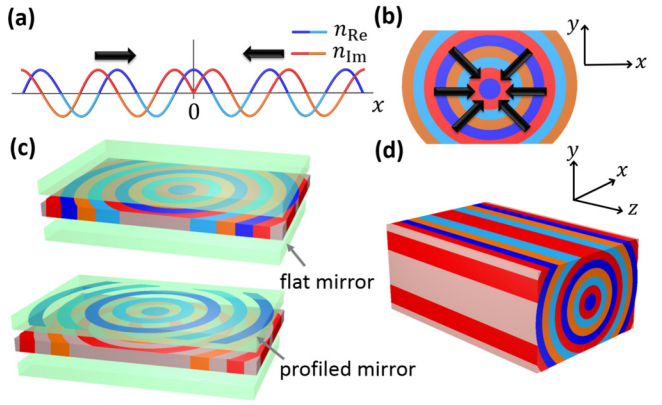

FIG. 1. Inward unidirectional coupling: (a) 1D complex potential, where n_{Re} and n_{Im} correspond to the real and imaginary parts of the modulation of the potential; (b) analogous axisymmetric configuration in 2D. (c) Two possible realizations of such 2D geometries in broad aperture microlasers (modified VCSELS) with either a modulated gain layer and/or a modulated (microcorrugated) mirror, with asymmetric spatial coupling of the fields evolving in time. (d) 3D coaxial complex modulation, analogous to (b) and (c), with asymmetric radial coupling for fields propagating along z. The arrows in (a) and (b) indicate the direction of the asymmetric mode coupling.

II. MODEL

We start with the general normalized paraxial electromagnetic field equation (equivalent to the Schrödinger equation for a quantum wave function) as a mathematical model, including diffraction and a complex potential, as

$$\partial_t A(r,t) = i\nabla_\perp^2 A(r,t) + iU(r)A(r,t), \tag{1}$$

where $A(r,t)$ is the slowly varying amplitude envelope of the complex electromagnetic field distributed in space, r, and $U(r)$ is the potential with a profile satisfying the particular symmetry conditions. The particular requirement for the potential is the local $\mathcal{PT}$ symmetry: $U(|r_0 + r|) = U^*(|r_0 - r|)$, with respect to periodically distributed points r_0, being $r_0 \neq 0$; and the global $\mathcal{P}$ symmetry: $U(r) = U(-r)$. For simplicity, using normalized spatial coordinates, such a potential may be expressed as $U(r) = n_{\mathrm{Re}}\cos(|x| + \phi) - in_{\mathrm{Im}}\sin(|x| + \phi)$ in 1D, and $U(r) = n_{\mathrm{Re}}\cos(r + \phi) - in_{\mathrm{Im}}\sin(r + \phi)$ in 2D as illustrated in Fig. 1. Here, n_{Re} and n_{Im} denote the normalized amplitudes of the real and the imaginary components of the potential, respectively. The phase ϕ characterizes the $\mathcal{P}$-symmetry center, at $r = 0$, being an important parameter for the field localization and enhancement. Therefore, n_{Re}, n_{Im}, and ϕ are the three key parameters determining the spatial and temporal dynamics of such systems. Equation (1) describes the field temporal evolution of the schemes represented in Figs. 1(a)–1(c), or equivalently, the spatial evolution for propagation along z for Fig. 1(d).

III. 1D SYSTEMS

We numerically solve Eq. (1) considering the general 1D potential $U(r) = n_{\mathrm{Re}}\cos(|x| + \phi) - in_{\mathrm{Im}}\sin(|x| + \phi)$, for an initial Gaussian beam: $A(x) = A_0 e^{-(x/w)^2}$ where the initial

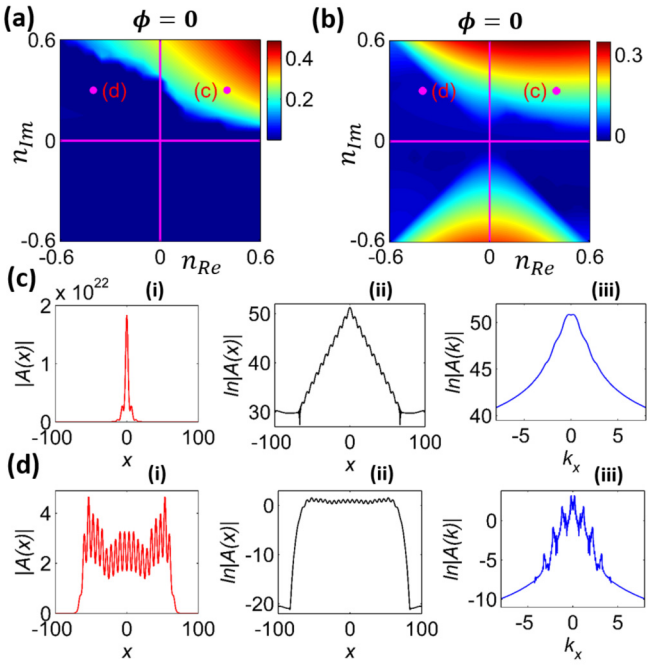

FIG. 2. 1D locally $\mathcal{PT}$-symmetric and globally $\mathcal{P}$-symmetric systems. (a) Localization (k_{Im}) map calculated after a sufficient long time ($t\sim$300 units) in parameter space (n_{Re},n_{Im}) for $\phi = 0$. (b) Growth (ω_{Im}) map at the center ($x = 0$) for $\phi = 0$ in the parameter space, obtained numerically with a finite difference time domain method using a hyper-Gaussian filter as boundary conditions. (c), (d) Analysis of two representative points, with parameter sets (0.4,0.3) and (−0.4,0.3), respectively. For both points, the spatial field profiles in linear and natural logarithmic scales are shown in (i) and (ii), while (iii) represents the spatial field spectra, as obtained from the Fourier transform, in natural logarithmic scale. Note that localization, k_{Im}, and growth, ω_{Im}, exponents are dimensionless quantities due to the normalization.

beam width w is broad enough to cover several $\mathcal{PT}$- modulation periods ($w \gg 1$). As expected, such a system develops an exponential field localization at $x = 0$, also exhibiting an exponential growth in time, due to the linear nature of the system. The envelope of the field may be asymptotically expressed as $A(x) \approx e^{-i\omega t}e^{-ik|x|}$ where $k = k_{\mathrm{Re}} + ik_{\mathrm{Im}}$ and $\omega = \omega_{\mathrm{Re}} + i\omega_{\mathrm{Im}}$ are both complex numbers; k_{Im} and k_{Re} denote the spatial localization exponent and wave number of a dominant mode, respectively, while ω_{Im},ω_{Re} stand for the temporal growth exponent and temporal oscillation frequency. We numerically obtain the localization as $k_{\mathrm{Im}} = d/dx(\ln[A(x,t)])$, after a sufficient long evolution time; and the temporal growth at $x = 0$ as: $\omega_{\mathrm{Im}} = d/dt(\ln[A(0,t)])$. We explore the parameter space (n_{Re},n_{Im}) to determine the regimes of maximum field localization and growth; the results are summarized in Fig. 2.

The field is expected to be localized around the $\mathcal{P}$-symmetry point for $n_{\mathrm{Re}} \approx n_{\mathrm{Im}}$, resulting from the unidirectional coupling between propagating waves, on the left-hand $x < 0$ and right-hand $x > 0$ half-spaces. The dark blue area in both maps represents almost no localization [Fig. 2(a)] or no field growth [Fig. 2(b)]. We observe that the growth for $\phi = 0$ is larger at the top and bottom regions [see Fig. 2(b)], suggesting that it

strongly depends on the amplitude of gain modulation, n_{Im}. More precisely, the growth attains large values for parameter sets with $|n_{\mathrm{Im}}| > |n_{\mathrm{Re}}|$ where the system displays a GLM-like behavior. However, on the top-right quadrant ($n_{\mathrm{Re}} > 0$, $n_{\mathrm{Im}} > 0$), for $\phi = 0$, the $\mathcal{P}$ symmetry and the presence of a higher index at $x = 0$ surrounded by gain areas, leads to large growths and strong localizations for large values of n_{Re} and n_{Im} values, indicating the crucial role of the interplay between the real and the imaginary modulations [Fig. 2(a)].

To illustrate the effect of the $\mathcal{PT}$ potential on the spatiotemporal field dynamics, we consider two representative points, (c) and (d), with the same gain-loss modulation but opposite sign in the index modulation profile, lying within and outside the field localization area. Note that while for point (c) the potential leads to an inward coupling of the wave vectors inducing a sharp field localization [see Fig. 2(c)(i)], the coupling at point (d) is outward and the field is spatially spread [see Fig. 2(d)(i)]. The same field profiles represented in logarithmic scale evidence the exponential character of the localization in Fig. 2(c)(ii), while localization is nearly zero for the flat curve of Fig. 2(d)(ii). We also provide both spatial field spectra in Figs. 2(c)/2(d)(iii) as obtained from the Fourier transform, although resonant peaks are not visible for point (c) due to the exponential slopes. Note that the spectrum in Fig. 2(c)(iii) extends over the first and second harmonics of the modulation. The effect of index and gain-loss modulation on field localization and enhancement, for $\phi = 0$, in parameter space, is also shown in Supplemental Material video 1 [21].

The localization is, however, remarkably phase dependent, occurring in different quadrants of the parameter space for different phases. Figures 3(a), 3(b), and 3(c) provide the localization maps for the representative phases: $\pi/4, \pi/2$, and π. Note that, while for $\phi = \pi/4$ localization also occurs for the first quadrant ($n_{\mathrm{Re}} > 0, n_{\mathrm{Im}} > 0$), a comparison with the map provided in Fig. 2(a) clearly indicates that the most intense field localization is achieved for $\phi = 0$. For $\phi = \pi/2$ strong localization flips to the second quadrant ($n_{\mathrm{Re}} < 0, n_{\mathrm{Im}} > 0$) where the system is almost PhC-like. Further increasing the phase, for $\phi = \pi$, localization moves on to the third quadrant ($n_{\mathrm{Re}} < 0, n_{\mathrm{Im}} < 0$) (being the corresponding map exactly symmetric to the one for $\phi = 0$). Supplemental Material video 2 visualizes how the localization regime spins counterclockwise when the phase increases. Localization is stronger when the asymmetric coupling between wave vectors provided by the local $\mathcal{PT}$-symmetric complex optical potential is directed inward [see the insets of Figs. 3(a) and 3(c)], being enhanced for larger gain-loss modulation amplitudes; these situations correspond to a GLM-like system. Note that strong localization is achieved around $x = 0$ due to the combined effect of local $\mathcal{PT}$ and global $\mathcal{P}$ symmetry. However, stand-alone $\mathcal{P}$ symmetry can also provide weaker localization for particular phases, e.g., localization at the $n_{\mathrm{Re}} = 0$ axis in Fig. 3(a). In addition, a small localization region is also found for $\phi = \pi/2$, indicating a PhC-like behavior, not relying on local $\mathcal{PT}$ symmetry, as coupling is directed outward in the case of Fig. 3(b).

A direct interpretation of the different localization regimes may be based on the competition of spatial modes in the field spectra. The interaction of different growing modes gives birth to different localization regimes, depending upon

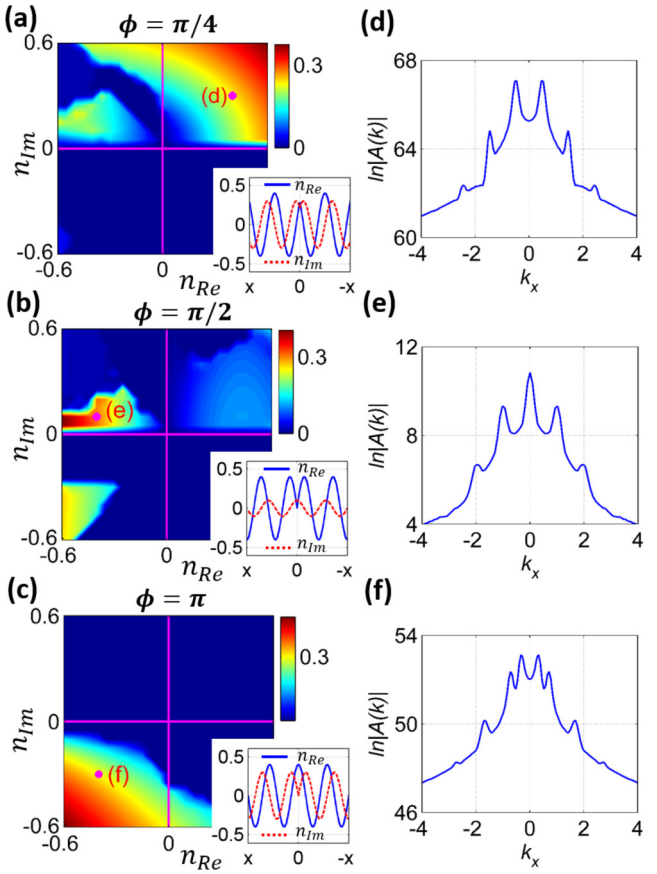

FIG. 3. Phase dependence and mode analysis in 1D systems. (a)–(c) Localization (k_{Im}) maps calculated after a sufficient long time ($t \sim 300$ units) in parameter space (n_{Re},n_{Im}) for $\phi = \pi/4, \pi/2$, and π, respectively. (d)–(f) Spatial field spectrum as obtained from the Laplace transform, in natural logarithmic scale, for representative points within the field localization areas for each phase corresponding to the parameter sets (0.4,0.3), (−0.4,0.1), and (−0.4,−0.3). The insets in localization maps (a)–(c) display the corresponding potential profiles for each representative point. The dominant modes, k_x, of the three representative points are: (d) $k_x = \pm 0.5, \pm 1.5, \pm 2.5, \ldots$; (e) $k_x = 0, \pm 1, \pm 2 \ldots$; and (f) $k_x \approx \pm 0.3, \pm 0.7, \pm 1.70, \ldots$.

the modulation amplitudes and phase. Since the spatial modes have an intrinsic complex nature, $k = k_{\mathrm{Re}} + ik_{\mathrm{Im}}$, the commonly used Fourier transform does not allow a precise localization of the real components of the spectrum, as growing modes have exponential slopes. In this situation, the Laplace transform is the optimal method to explore the complex spectrum [22]. The Laplace transform defined as $A(s) = \int_0^\infty A(x)e^{-sx}dx$ is a generalization of the Fourier transform, since being $s = \sigma + ik$, it reduces to the Fourier transform for $\sigma = 0$. For a decaying field in the form $A(x) = e^{-(ik_{\mathrm{Re}} - k_{\mathrm{Im}})x}$, the Fourier and Laplace transforms result, respectively, as $A(k) = 1/[k_{\mathrm{Im}} + i(k_{\mathrm{Re}} - k)]$ and $A(s = \sigma + ik) = 1/[(k_{\mathrm{Im}} - \sigma) + i(k_{\mathrm{Re}} - k)]$. This Laplace transform has a pole at $(\sigma,k) = (k_{\mathrm{Im}},k_{\mathrm{Re}})$ and the cross section over the pole $\sigma = k_{\mathrm{Im}}$ gives a sharp peak. We obtain the Laplace transform numerically, which however is defined on the half plane, $k_{\mathrm{Im}} \geqslant \sigma$ and provide its cross section for $k_{\mathrm{Im}} \approx \sigma$, where σ is calculated from the field localization exponent in Figs. 3(d)–3(f) for

particular parameter sets. We essentially identify three distinct regimes on the basis of symmetric spatial modes participating in the field spectrum. The simplest case corresponds to the PhC-like limit, where a set of dominant integer modes $k_x = 0,\pm1,\pm2,\ldots$ prevail in the spatial spectrum [see Fig. 3(b) for $\phi = \pi/2$]. The other two localization regimes correspond to the GLM-like limit. In a pure GLM system, the spectrum shows frequency peaks centered at $\pm0.5,\pm1.5,\pm2.5,\ldots$; this is the case for $\phi = \pi/4$ [see Fig. 3(a)]. However, large gain-loss modulation amplitudes lead to a strong coupling between different harmonics, eventually shifting the central frequency peaks towards lower wave numbers, e.g., the system dynamics supports the dominant mode set $k_x \sim \pm0.3,\pm0.7,\pm1.7$, for $\phi = 0,\pi,\ldots$ in Fig. 3(c).

IV. 2D SYSTEMS

Next, we proceed to analyze local $\mathcal{PT}$ symmetry and global $\mathcal{P}$ symmetry in 2D, considering the axisymmetric potential: $U(r) = n_{\mathrm{Re}}\cos(r+\phi) - in_{\mathrm{Im}}\sin(r+\phi)$. The results for $\phi = 0$ are summarized in Fig. 4. Analogously to the 1D potential, a field enhancement is found at the center, $r = 0$, now attributed to the asymmetric radial coupling between inward and outward propagating waves. Figure 4(a) provides the localization obtained from the correspondingly linearized field. Since the axial cross-sectional profile of the field [see Fig. 4(c)(v)] is not exponentially decreasing, due to the $1/r$ factor of the axial symmetry, localization is obtained from the exponential slope of $A(r)\sqrt{r}$ [see Fig. 4(c)(vi)]. The top-right side of the map, $(n_{\mathrm{Re}} > 0, n_{\mathrm{Im}} > 0)$, exhibits the more intense field localization area, approximately corresponding to the one obtained in 1D in Fig. 2(a). This result, along with the central growth map for $r = 0$, provided in Fig. 4(b), indicates that the overall scenario resembles the 1D situation. The field profile shows a sharp peak in the 2D plane for the parameter set of point (c) laying within the localization range [see Figs. 4(c)(i) and 4(c)(iv)]. Additionally, Figs. 4(c)(iii) and 4(c)(vii) depict the phase of the field in which the slope increases with jumps from $-\pi$ to $+\pi$, clearly showing the inward propagation. While remaining analogous to 1D, the proposed effect in this 2D case is more realistic and opens new avenues in optics for extraordinary field confinement and high power density at a selected position. In addition, since the beam shaping effect relies on the anisotropic amplification of modes with small wave vectors it is robust against noise, contrary to the conventional mechanism of filtering out nondesired modes, with higher wave vectors. Next, we provide an example to demonstrate the functionality of our proposal in a nonlinear regime.

V. APPLICATION TO VCSELs

Broad aperture lasers, and VCSELs among them, are relevant laser sources; however, they suffer from a major drawback of poor beam quality due to the lack of an intrinsic transverse mode selection mechanism. In lowest approximation, the field dynamics of VCSELs with the proposed complex potential profile, $U(r)$, satisfying the particular symmetry conditions in either the 1D or the 2D axisymmetric case, can be described

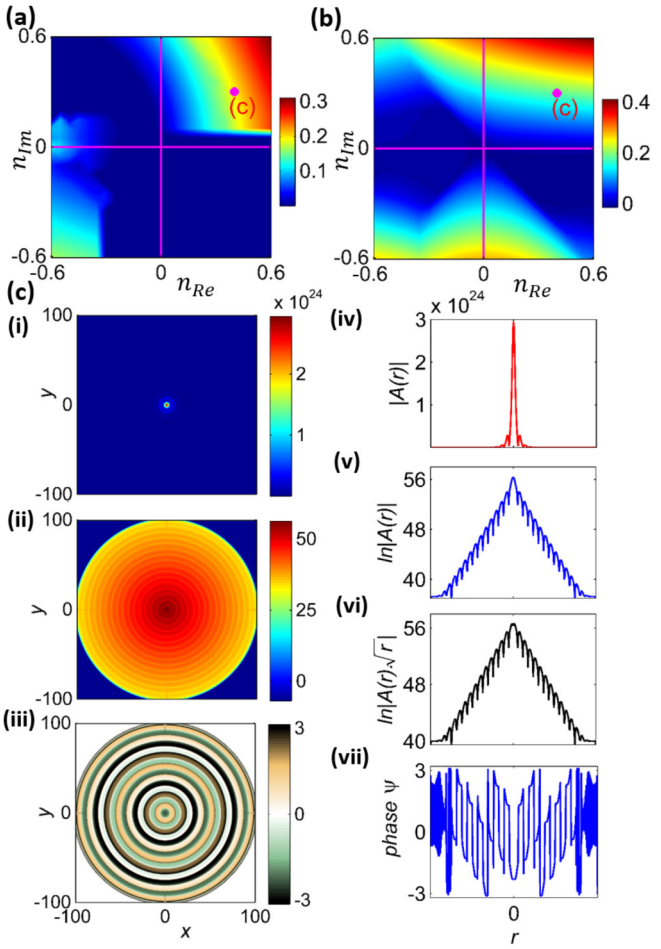

FIG. 4. (a) Localization (k_{Im}) map of the axial cross-section profile of the field linearized as $A(r)\sqrt{r}$ for a 2D $\mathcal{PT}$-axisymmetric system as in Fig. 1(b), calculated after sufficient long time ($t \sim 300$ units) in parameter space ($n_{\mathrm{Re}}, n_{\mathrm{Im}}$). (b) Growth ($\omega_{\mathrm{Im}}$) map of the center ($r = 0$) in parameter space. A strong field enhancement and localization at $r = 0$ is shown in (c) for the parameter set (0.4,0.3). (i), (ii) 2D spatial field profiles in linear and natural logarithmic scales, respectively. (iii) Field phase. Panels (iv), (v), and (vii) display the axial cross-sectional profiles of (i)–(iii), while (vi) depicts the linearized field, $A(r)\sqrt{r}$, in natural logarithmic scale.

by a complex Ginzburg-Landau equation [23]:

$$\partial_t A(r,t) = (p - |A|^2)A + i\nabla_\perp^2 A(r,t) + iU(r)A(r,t), \quad (2)$$

where $A(r,t)$ is the envelope of complex field distributed in space, r, and p is pump parameter. The nonlinearity is due to gain saturation. The complex potential profile, $U(r)$, satisfies the local $\mathcal{PT}$-symmetry and global $\mathcal{P}$-symmetry conditions for 1D and 2D axisymmetric systems as discussed above. Such nonlinear systems generally show the saturation phenomena with uniform field distribution for $p > 0$. However, the field localization and enhancement in such situation is possible at the center for $p < 0$ by applying locally $\mathcal{PT}$-symmetric and globally $\mathcal{P}$-symmetric potential. The results for a particular parameter set are provided in Fig. 5. The spatial field profile showing the concentration at the center, $r = 0$, in Fig. 5(a), reveals that the 2D $\mathcal{PT}$-axisymmetric system efficiently localizes the field also in the nonlinear regime.

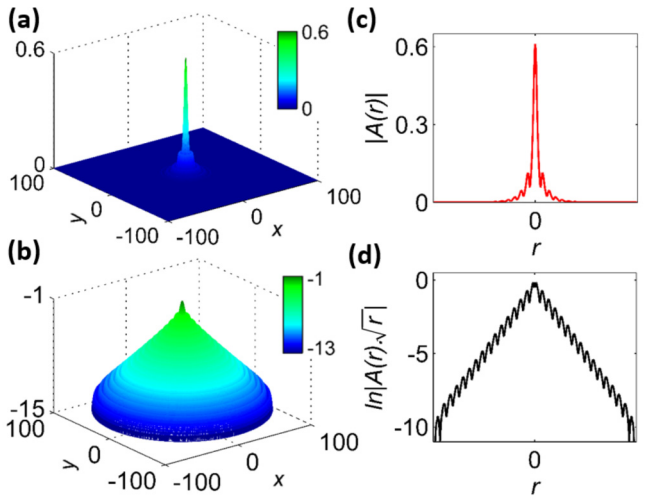

FIG. 5. Spatial field distributions for a 2D $\mathcal{PT}$-axisymmetric VCSEL, calculated after the steady state ($t\sim$150 units) for $p = -0.1$ and parameter set (0.4,0.4). 3D visualization of the VCSEL output field profile, concentrated and enhanced at $r = 0$ in linear (a) and natural logarithmic (b) scales. (c), (d) Axial cross-sectional profile of the field in linear and natural logarithmic scale.

VI. CONCLUSIONS

To conclude, we propose a class of local $\mathcal{PT}$-symmetric and global $\mathcal{P}$-symmetric systems providing a unique platform for extreme field localization and enhancement around the $\mathcal{P}$-symmetry point. We provide an alternative to conventional localization mechanisms, different from the classical index guiding (trapping potential), gain guiding, and other systems commonly based on Bragg gratings or gain gratings (distributed feedback). In the proposed scheme, field concentration is achieved by asymmetric radial coupling of inward and outward waves, to which both index and gain-loss contribute simultaneously to the localization of the field. Specifically, this class of systems can strongly localize the field, depending on the relative modulation amplitudes and phase of the complex potential. Therefore, the most interesting scenario occurs for GLM-like systems, for which extreme field concentrations are achieved for a wide range of parameter sets, for $\phi = 0$, either in the proposed 1D or 2D axisymmetric configurations. Also for PhC-like systems, less significant field localizations are obtained for some particular potential phases. It is also worth mentioning that all potentials satisfying local $\mathcal{PT}$-symmetry and global $\mathcal{P}$-symmetry conditions can provide the same localization irrespective of some specific potential profile. Such potentials could be designed in a variety of different ways to observe the proposed effect, e.g., sawtooth and stepwise potentials with equation $U(x) = \sum 1/n \exp(inqx)$ where $n = 1,2,3,\ldots$ or $n = 1,3,5,\ldots$, respectively.

The fundamental concept may also be easily implemented to find remarkable applications in various linear and nonlinear optoelectronic devices where a high degree of localization is essentially desirable such as optical switching in nanostructures, optical modulators, or broad aperture lasers and microlasers. In particular, we show a possible direct application for an axially modulated VCSEL to improve the brightness and quality of beam emission to show its applicability in particular implementations. We note the universality of this nonlinear example as based on a general complex Ginzburg-Landau equation, confirming that the field localization and concentration at around the point of merging of two symmetries can be realized in other different physical systems in Bose condensates and acoustics, among others.

We acknowledge financial support by Spanish Ministerio de Educación y Ciencia through project FIS2015-65998-C2-1-P, by NATO under Grant No. SPS-985048, and by Erasmus Mundus Doctorate Program Europhotonics under Grant No. 159224-1-2009-1-FR-ERA MUNDUS-EMJD.

[1] C. M. Bender and S. Boettcher, Phys. Rev. Lett. **80**, 5243 (1998).
[2] C. M. Bender, Rep. Prog. Phys. **70**, 947 (2007).
[3] X. Zhu, H. Ramezani, C. Shi, J. Zhu, and X. Zhang, Phys. Rev. X **4**, 031042 (2014).
[4] H. Benisty, A. Degiron, A. Lupu, A. De Lustrac, S. Chénais, S. Forget, M. Besbes, G. Barbillon, A. Bruyant, S. Blaize, and G. Lérondel, Opt. Express **19**, 18004 (2011).
[5] D. Haag, D. Dast, H. Cartarius, and G. Wunner, Phys. Rev. A **92**, 053627 (2015).
[6] A. Guo, G. J. Salamo, D. Duchesne, R. Morandotti, M. Volatier-Ravat, V. Aimez, G. A. Siviloglou, and D. N. Christodoulides, Phys. Rev. Lett. **103**, 093902 (2009).
[7] C. E. Ruter, K. G. Makris, R. El-Ganainy, D. N. Christodoulides, M. Segev, and D. Kip, Nat. Phys. **6**, 192 (2010).
[8] A. Regensburger, C. Bersch, M. A. Miri, G. Onishchukov, D. N. Christodoulides, and U. Peschel, Nature (London) **488**, 167 (2012).
[9] S. Longhi, J. Phys. A: Math. Theor. **44**, 485302 (2011).
[10] Z. Lin, H. Ramezani, T. Eichelkraut, T. Kottos, H. Cao, and D. N. Christodoulides, Phys. Rev. Lett. **106**, 213901 (2011).
[11] L. Feng, Y.-L. Xu, W. S. Fegadolli, M.-H. Lu, J. E. Oliveira, V. R. Almeida, Y.-F. Chen, and A. Scherer, Nat. Mater. **12**, 108 (2012).
[12] S. Longhi, Phys. Rev. A **82**, 031801 (2010).
[13] Y. D. Chong, L. Ge, and A. D. Stone, Phys. Rev. Lett. **106**, 093902 (2011).
[14] K. Hirose, Y. Liang, Y. Kurosaka, A. Watanabe, T. Sugiyama, and S. Noda, Nat. Photonics **8**, 406 (2014).
[15] H. Hodaei, M. A. Miri, M. Heinrich, D. N. Christodoulides, and M. Khajavikhan, Science **346**, 975 (2014).
[16] K. Iga, IEEE J. Sel. Top. Quantum Electron. **6**, 1201 (2000).
[17] K. Staliunas, R. Herrero, and R. Vilaseca, Phys. Rev. A **80**, 013821 (2009).
[18] M. Botey, R. Herrero, and K. Staliunas, Phys. Rev. A **82**, 013828 (2010).
[19] R. Herrero, M. Botey, M. Radziunas, and K. Staliunas, Opt. Lett. **37**, 5253 (2012).

[20] M. Radziunas, M. Botey, R. Herrero, and K. Staliunas, Appl. Phys. Lett. **103**, 132101 (2013).

[21] See Supplemental Material at http://link.aps.org/supplemental/10.1103/PhysRevA.94.053819 for the visualization of the field localization and enhancement around the $\mathcal{P}$-symmetry center. Video 1 shows the effect of the index and gain-loss modulation amplitudes on the field localization and growth, for $\phi = 0$; the potential and field profiles are provided, after a sufficient propagation time, for different points along a circular path in the parameter space $(m_{\mathrm{Re}}, m_{\mathrm{Im}})$. Video 2 shows the dependence of the localization and growth regimes on the phase of the locally $\mathcal{PT}$-symmetric and $\mathcal{P}$-symmetric potential; the strongest localization area spins counterclockwise on the parameter space $(m_{\mathrm{Re}}, m_{\mathrm{Im}})$, by increasing the phase from 0 to 2π.

[22] P. Moreno and A. Ramirez, IEEE Trans. Power Delivery **23**, 2599 (2008).

[23] W. W. Ahmed, S. Kumar, R. Herrero, M. Botey, M. Radziunas, and K. Staliunas, Phys. Rev. A **92**, 043829 (2015).